doi:10.1038/nature10974

1. Sr_2CuO_3 compound

Sr_2CuO_3 is built up of CuO_4 plaquettes, arranged in chains with two plaquettes sharing a corner oxygen atom (fig. S1). The central atom of each plaquette contains a Cu ion in $3d^9$ configuration, corresponding to a hole (called 'particle' throughout the paper, see Sec. 2) in the 3*d* shell that carries a spin s=½. Due to the large on-site Coulomb repulsion *U* between the Cu 3*d* electrons, a Mott-insulating state arises. The optical gap of about 1.5 eV is of charge-transfer type, i.e. due to transfer of O *2p* electrons to the Cu *3d* shell. The large crystal-field anisotropy of the quasi 1D system leads to a ferro-orbital ground state, where the particles occupy on each plaquette Cu 3*d* x^2-y^2 orbitals. The AF superexchange coupling *J* between spins on neighbouring plaquettes is with *J*~250 meV exceptionally large[19,22] giving Sr_2CuO_3 the nearly ideal properties of a 1D AF spin-½ Heisenberg chain.

2. Particle-hole transformation

As mentioned in Sec. 1 above, the Cu^{2+} ion in Sr_2CuO_3 has 9 electrons in the 3*d* shell. Therefore, it is useful to make an electron-hole transformation and to discuss the physics of this compound in the 'hole' language: thus, as already pointed in Sec. 1, in the ground state there is only one hole in the 3*d* x^2-y^2 orbital so that, e.g., 'making an *xy* orbital excitation' corresponds to moving a hole from the x^2-y^2 to the *xy* orbital. However, we refer to these holes as 'particles' in the article, in order to avoid confusion with 'holes' defined throughout the paper as empty sites in the AF chain (which are in fact made up of two holes in the 'hole' language).

We implicitly use the 'hole' language to describe Sr_2CuO_3 in the paper, except for the four introductory paragraphs of the main text [including Fig. 1a-b] and for Sec. 3 with fig. S3 in this supplementary information (where in both cases it is much more customary to use the electron picture).

3. RIXS scattering process for orbital excitations

Resonant inelastic X-ray scattering (RIXS) is a photon-in photon-out technique for which choosing the appropriate incident photon energy to the absorption resonance tremendously enhances the cross section for specific excitations[9]. The measured photon energy transfer $\Delta E = h\nu_{in} - h\nu_{out}$ and momentum transfer $\boldsymbol{q} = \boldsymbol{k}_{in} - \boldsymbol{k}_{out}$ in a RIXS experiment is directly related to the energy and momentum of the created excitations (spinons, orbitons). For soft X-rays around 930 eV it is possible to probe $\boldsymbol{q}$ of the order of the size of a Brillouin Zone of Sr_2CuO_3.

An orbital excitation in the RIXS scattering process is illustrated in fig S3[*]. When the photon energy is tuned to the Cu L_3 edge, in the intermediate state the $3d$ x^2-y^2 orbital is occupied with two electrons, creating at the same time a $2p$ core hole in the j=3/2 state. In the following decay process the core hole can be refilled from a $3d$ orbital with a different symmetry, e.g. xz. Each transition has to obey the electric dipole (E1) selection rules, leading to specific polarization dependencies. In general, transitions of an electron are allowed from, e.g., xz to the x^2-y^2 orbital, either with spin up, spin down, or flipping an up (down) spin to down (up), each with a different resonant enhancement and

[*] Unlike in the rest of the paper, where the 'hole' picture is used, in this section we use the 'electron' picture to stay in agreement with Ref. 9.

polarization dependence. Local effective RIXS operators were derived for Cu d^9 by Luo et al.[12] and Van Veenendaal[30].

4. Further experimental details

The set up of our experiment is depicted in fig. S1 (for description see Methods summary and Methods). The variation of the projection of the incident-photons' polarization vector $\boldsymbol{\varepsilon}_{\text{in}}$ in the [100] and [010] directions, resulting from sample rotation for $\boldsymbol{q}$-dependent measurements, is shown in fig. S2b. The momentum transfer along the chains, q_a, is denoted with q in the main text and below.

5. Calculating the energies of Cu 3*d* orbitals using quantum chemistry *ab-initio* calculations

To acquire better insight into the Cu 3*d*-level electronic structure of Sr_2CuO_3 and the nature of the orbital excitations quantum chemical calculations were performed. In the spirit of modern multiscale electronic-structure approaches, we describe a given region around a central Cu site by advanced *ab initio* many-body techniques, while the remaining part of the solid is modeled at the Hartree-Fock level. The complete-active-space self-consistent-field (CASSCF) method was used to generate multireference wavefunctions for further configuration-interaction (CI) calculations, see e.g. Ref. 31. In the CASSCF scheme a full CI is carried out within a limited set of "active" orbitals, i.e., all possible occupations are allowed for those active orbitals. The active orbital set includes here all 3*d* functions at the central Cu site and the 3*d* x^2-y^2 functions of four Cu nearest neighbours. Strong correlations among the 3*d* electrons are thus accurately described. The multireference CI (MRCI) calculations incorporate on top of the

CASSCF wavefunction all single and double excitations from the Cu 3*s*, 3*p*, 3*d* and O 2*p* orbitals on a given CuO_4 plaquette and from the 3*d* x^2-y^2 orbitals of the four Cu nearest neighbours. To the MRCI energies we also added Davidson corrections that account for quadruple excitations in the CI expansion, see Ref. 31. Further technical details are discussed in Methods and in Ref. 19. It turns out by MRCI that the lowest crystal-field excitation at 1.62 eV is to the *xy* level. Excitations to the *xz* and *yz* orbitals require 2.25 and 2.32 eV, respectively, while the splitting between the x^2-y^2 and $3z^2$-r^2 levels is 2.66 eV. These values were computed for a ferromagnetic cluster, i.e., they do not include the effect of superexchange interactions in Sr_2CuO_3 (which would shift the energies by ca. ~ *J*). The results are tabulated in Table 1. Finally, let us note that we obtain a quantitative similar result using LDA Wannier orbitals[32,33] combined with multiplet ligand field theory.

	xy	*xz*/*yz*	$3z^2$-r^2
Experiment	1.85	2.36	2.98
Theory	1.62	2.25/2.32	2.66

Table 1 | Comparison between experimental and theoretical values (quantum chemistry cluster calculations) of on-site orbital excitations.

6. Ruling out competing scenarios to the J_O-J –model

The structure factor $O(q,\omega)$ (see Methods) reproduces correctly the experimental results. If one assumes that $O(q,\omega)$ is equal to unity also for the "dispersive" orbital excitations (*xz* and *xy*), then the result (fig. S4, left) cannot properly reproduce the experimental RIXS cross section. In other words, the observed orbital dispersion cannot be attributed

to a mere shift of spectral weight. In fact, this single ion picture[9-10] does not even correctly predict the intensity of the excitations: for example for the *xy* orbital excitation it suggests that it does not depend on momentum and thus it can only be the spin-orbital separation mechanism transferring the weight from the orbiton to the spinon-orbiton continuum.

Also a non-interacting band picture cannot explain the π periodicity of the spectrum, nor can it explain a large incoherent spectrum. We have also calculated the spectral function $O(q,\omega)$ using the mean-field decoupling of spin and orbitals [see e.g. Ref. 23] and then by calculating the orbiton dispersion similarly as in linear spin wave theory; in such a mean-field approach the hopping of the orbital excitation is by definition (and artificially) decoupled from the spin excitation. The impact of the spin background is in this case only reflected in a renormalization of J_O. Therefore, spin-orbital separation is absent and the spectral function of a particular orbital excitation (*xy* or *xz*) consists of a single dispersive quasiparticle peak with period 2π. As shown in the right panel of fig. S4, such results do not reproduce the experiment and indeed the exact diagonalization of the Hamiltonian H is needed to correctly reproduce the experimental results and in particular the observed π periodicity. Moreover, the particular shape of the RIXS cross section is due to the spin-orbital separation which cannot be captured by a mean-field approach.

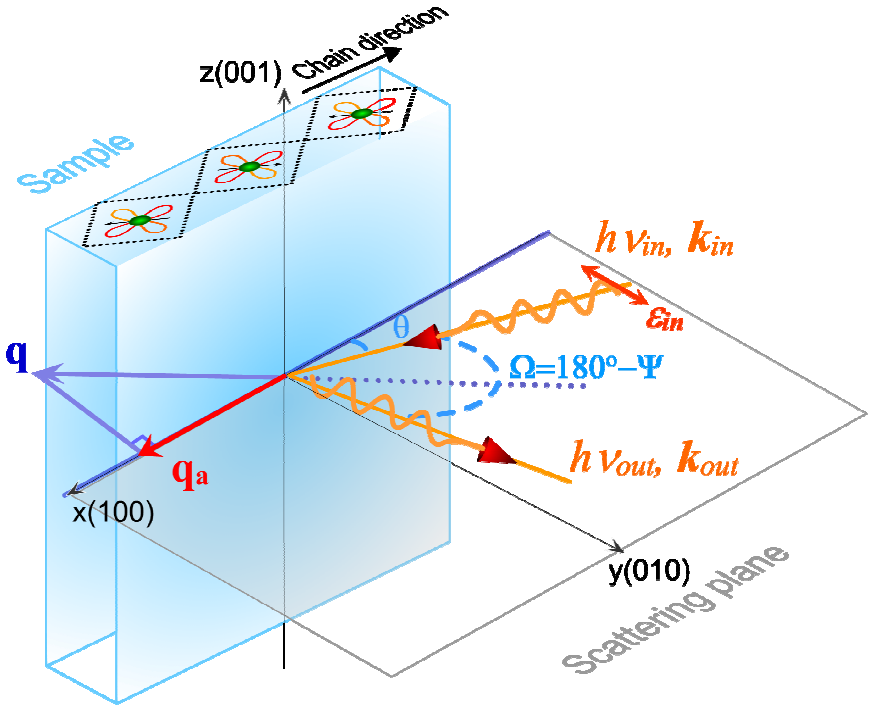

Figure S1 | Experimental geometry. Experimental geometry in our RIXS set up, see text for details. The orientation of the chains in Sr_2CuO_3 – built up from corner-sharing CuO_4 plaquettes (see also Fig. 1d main text) is shown: the green dots indicate the position of the Cu-sites with the lobes representing $3d\ x^2$-y^2 orbitals.

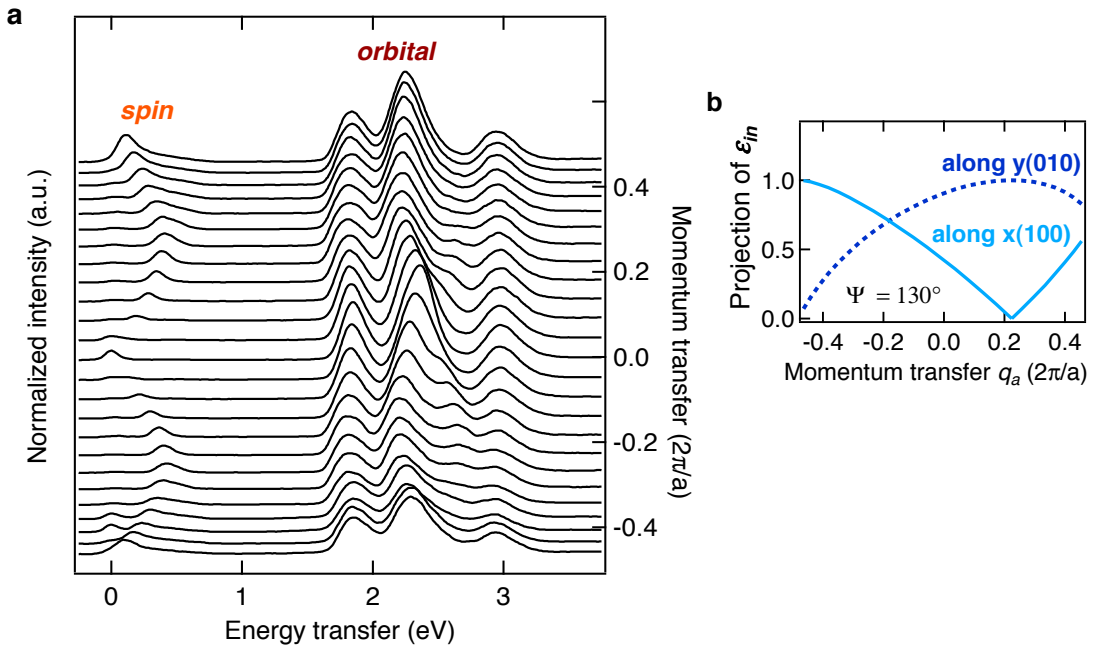

Figure S2 | RIXS line spectra and polarization dependence. a, RIXS line spectra for Ψ=130° (the same data set as the intensity map in Fig. 1c, main text). **b,** change of projection of the polarization vector of incoming photons, $\boldsymbol{\varepsilon}_{in}$, along the crystallographic directions (100) and (010), which is related to rotation of the sample for momentum-dependent measurements (Ψ=130°). See text for details.

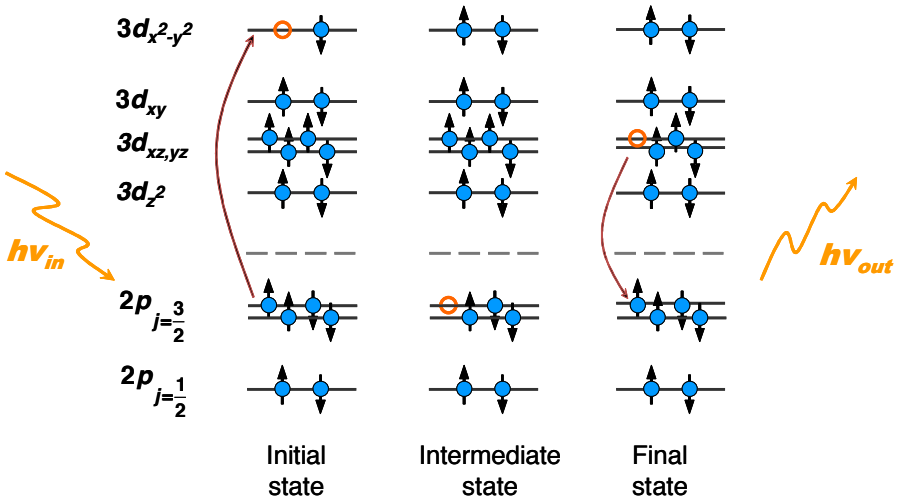

Figure S3 | RIXS scattering process for orbital excitations. Creation of an *xz* orbital excitation on a Cu^{2+} ion. Note that here for clarity the 'electron' picture is used – in contrast to the rest of the paper where the 'hole' picture is used.

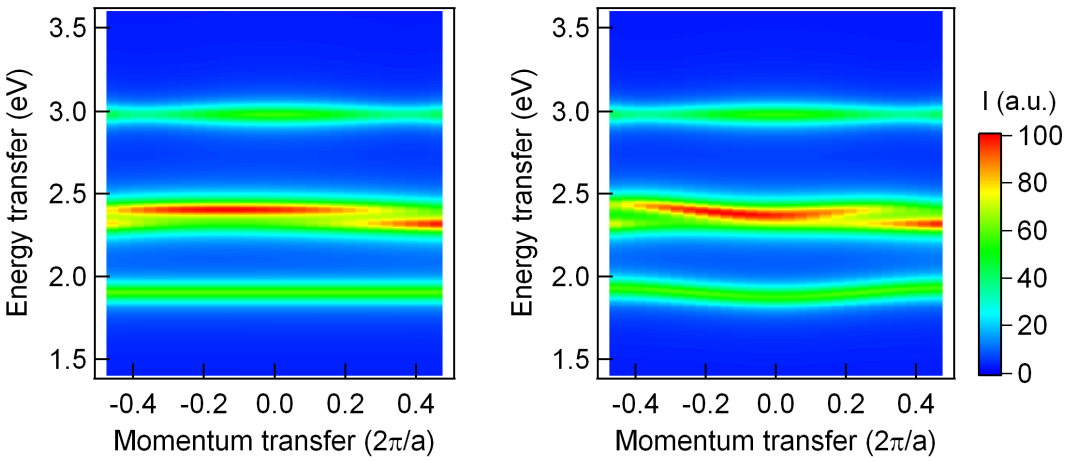

Figure S4 | Ab-initio calculations: alternative scenarios to the spin-orbital separation process. Simulation of the experimental data with the single-ion cross section (left) and with the linear orbital wave theory (right).

References

31. Helgaker, T. Jørgensen, P. and Olsen, J. Molecular Electronic-Structure Theory (Wiley, Chichester, 2000).

32. Pavarini, E. Dasgupta, I. Saha-Dasgupta, T. Jepsen, O. and Andersen, O. K. *Phys. Rev. Lett.* **87**, 047003 (2001).

33. Haverkort, M. W. Zwierzycki, M. Andersen O. K. *arXiv:* 11114940 (2011).